Self-reference extended depth-of-field quantitative phase microscopy

Jaeduck Jang[a], Chae Yun Bae[b], Je-Kyun Park[b], and Jong Chul Ye[a]

[a]Bio Imaging & Signal Processing Laboratory, Department of Bio and Brain Engineering, KAIST, Gwahangno 335, Daejeon, Republic of Korea;
[b]NanoBiotech Laboratory, Department of Bio and Brain Engineering, KAIST, Gwahangno 335, Daejeon, Republic of Korea

ABSTRACT

This paper describes a novel quantitative phase microscopy based on a simple self-referencing scheme using Michelson interferometry. In order to achieve the homogeneous reference field for accurate phase measurement, the imaging field-of-view (FOV) is split onto the sample and homogenous background areas. The reference field can be generated by rotating the relative position of the sample and homogenous background in the object arm. Furthermore, our system is realized using an extended depth-of-field (eDOF) optics, which allows quantitative phase measurement for an increase of the depth-of-field without moving objective lens or specimen. The proposed method is confirmed by experimental results using various samples such as polystyrene beads and red blood cells (RBCs).

Keywords: cell analysis, microscopy, phase imaging

1. INTRODUCTION

Phase microscopy is commonly used to visualize transparency samples without the assistance of exogenous contrast agent. Due to inhomogeneous refractive index in the sample and background, the phase information reflects the optical path length (OPL) of the transmitted light through a sample. Phase contrast (PhC) and differential interference contrast (DIC) have traditionally been used to obtain phase contrast by changing OPL using specialized optical components. For example, the phase contrast (PhC) microscopy introduced by Zernike[1] utilizes the phase plate which is mounted at the back focal plane of the objective lens to enhance the difference of the scattered and unscattered light. Moreover the differential interferometry contrast (DIC) microscopy introduced by Nomarski[1] applies the interfered phase difference between two polarized light by use of Wollaston prisms placed at illumination and detection optics. At illumination optics, Wollaston prism is placed at the front focal plane of the condenser lens, and splits the incident light into s- and p-polarized beams which have slightly different beam paths on the specimen by a condenser lens. Finally the split beams are combined at the back focal plane of the objective lens by the 2nd Wollaston prism. Since the s- and p-polarized light have slightly different OPL, the combined and interfered light transforms the difference of refractive index or thickness property into a contrast image. However, these types of conventional phase microscopy fail to measure the quantitative phase image.

Recently, several quantitative phase microscopes (QPM) have been extensively applied in biological research areas.[2–6] Fourier phase microscopy (FPM) applies the principle of PhC microscopy and phase shifting interferometry (PSI).[2] The programmable phase modulator (PPM) is used to control the phase of the scattered light from a sample with respect to unscattered light. In the case of Hilbert phase microscopy (HPM), the optical system delivers light using an optical fiber to minimize the phase noise, and Hilbert transform reconstruction improves the temporal resolution up to a few milliseconds using a single interferogram recording.[3] Surface plasmon resonance (SPR) technique is also integrated with QPM to quantify the phase profile of DNA microarray.[7]

Further author information: (Send correspondence to J.C. Ye)
J.C. Ye: E-mail: jong.ye@kaist.ac.kr, Telephone: +82 (42) 350 4320
J. Jang: E-mail: shyboy3@kaist.ac.kr, Telephone: +82 (42) 350 4360

Three-Dimensional and Multidimensional Microscopy: Image Acquisition and Processing XVII, edited by Jose-Angel Conchello, Carol J. Cogswell, Tony Wilson, Thomas G. Brown, Proc. of SPIE Vol. 7570, 757018
 · doi: 10.1117/12.843082

Digital holographic microscopy (DHM) allows three dimensional imaging based holography.[5] Many QPMs generate interferograms using an isolated reference field from non-scattered light through separate optical paths. To remove heterogeneous phase noise due to distinct beam paths, diffraction phase microscopy (DPM)[6] splits a specimen image with a diffraction grating through which the first order diffracted field becomes the object field, whereas the zeroth order field is used as the reference field.

In this paper, we develop a novel self-reference interferometry especially suitable for monitoring microfluidic devices. Our system uses the light through the non-channelized areas of microfluidic devices as a reference field. More specifically, using Michelson interferometry, incident beams through the channel and non-channel areas are split onto the reference and the object arms (Figs. 1(a)(b)). Unlike conventional Michelson interferometry, the 2nd objective lens is used for imaging inversion optics in the object arm. Since the reference arm and the object arm switch the relative position of the specimen and the homogeneous background, a double interferogram can be obtained, as shown in Fig. 1(c). Two distinct setups, PSI and HPM, can be readily implemented by changing the reflection optics in the reference arm. In the PSI setup, a reflection type SLM (Spatial Light Modulator) controllably shift the phase of the reference fields (Fig. 1(a)). The main advantage is to replace the scanning of the objective lens or the specimen with a mirror scanning in the object arm to facilitate the increase of the depth-of-field.[8] This increased depth-of-field is especially important in such applications with limited working distance between objective lens and specimen. In the HPM setup, a simple mirror is used instead of SLM (Fig. 1(b)). Since our setups form double interferograms simultaneously, a higher signal-to-noise ratio (SNR) phase map can be obtained by averaging the two phase reconstructions. Even though our system has the limitation of smaller field-of-view (FOV), it is still suitable for monitoring microfluidic devices since microfluidic devices usually have a wide non-channelized area compared with the microchannel.

2. MATERIAL AND METHODS

The optical system in the proposed method is based on the modified Michelson interferometry using eDOF optics. Figure 1(a)(b) illustrate PSI and HPM setups, respectively. The He-Ne laser is used as an illumination source. The 40× (0.55 NA) and 100× (1.30 NA) microscope objective lenses are used at MO1. The magnified specimen image by MO1 is delivered by 4f optics by L1 ($f_1 = 200mm$) and L2 ($f_2 = 200mm$). For a large depth-of-field, the 2nd tube lens (L2) and the 2nd objective lens (MO2, 20×, $NA = 0.50$) are located at symmetric positions of L1 and MO1 with respect to FP plane. According to previous literature,[9] these optics reduces the spherical aberration of an objective lens. The magnified specimen image through L2 is splits onto the reference arm and the object arm. Depending on the PSI and HPM setups, we placed SLM in Fig. 1(a) and a simple mirror (M4) in Fig. 1(b), respectively. In PSI setup, we control the uniform gray level image on SLM (LC-R 2500, Holoeye) using external computer interface, and the phase of incident light is between $0 \sim 2\pi$ with 8 bit resolution. Additionally, polarizer (P) and analyzer (A) support the phase modulation mode of SLM. SLM rapidly changes the phase of incident light at 60Hz. In HPM setup, a simple mirror reflects the incident light without changing of phase. Compared with an image (I_R) from the reference arm in Fig. 2(a), the position of the polystyrene bead in Fig. 2(b) is the rotated position of the Fig. 2(a). The combined beam from Fig. 2(a)(b) forms double interferogram as shown in Fig. 2(c). Using Hilbert transformation with high pass filtering, we acquire two phase reconstructions with double interferogram. The spatial modulation frequency of an interferogram is controlled by the incident angle of two light from each arm. We applied the CMOS digital camera (Canon, 450D) at the detector plane using adaptor lens (L3, $f_3 = 200mm$).

2.1 Extended Depth-of-field

From the Figs. 1(a)(b), a pair of microscope objective lens with tube lens is applied to increase the depth-of-field. Note that the optical system compensates for the spherical aberration stemming from the high numerical aperture (NA) objective lens due to the eDOF microscopic principle.[9] In the case of the high NA objective lens, the spherical aberration mainly originates from the pupil function of the lens, which has a low depth-of-field, i.e., $DOF \approx n\lambda/NA^2$. The objective lens with the tube lens generally satisfies the Sine condition[9] that allows transformation of the focal plane of the objective lens to the back focal plane of the tube lens without aberration. Additionally, an optical system is called to satisfy the Herschel condition, if it allows the objects along the optical axis to be exactly reproduced. Recent research has demonstrated that the perfect imaging system, satisfying

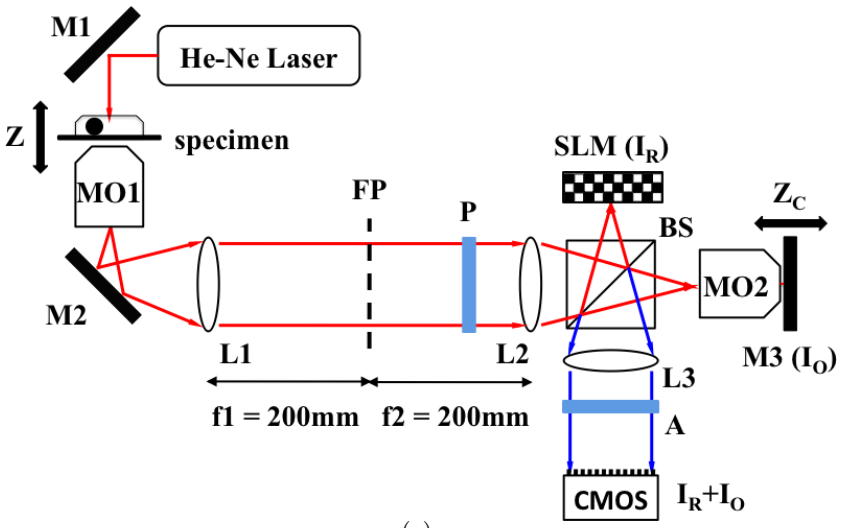

(a)

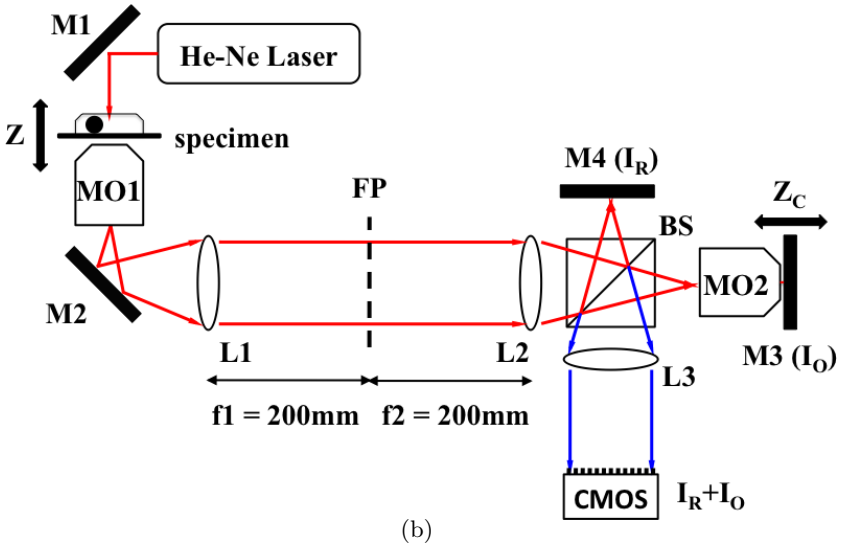

(b)

Figure 1. Diagram of the PSI and HPM optical systems: (a), (b) PSI and HPM optical setups, respectively; I_O reflected from M3 is an inverted image of I_R, which is reflected from SLM and M4 for PSI and HPM, respectively. Therefore, the total measurement fields at the detector corresponds to the summation of two, which produces the double interferogram.

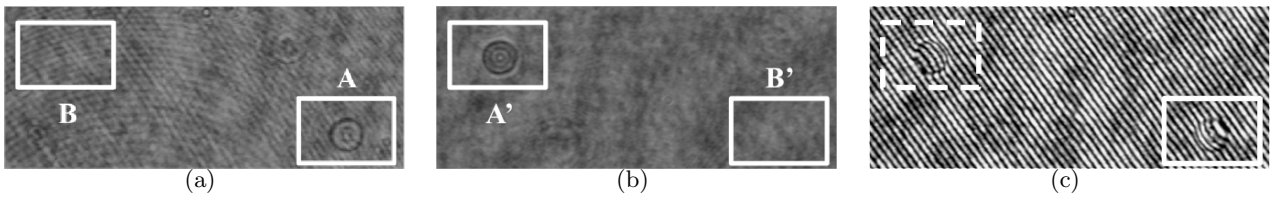

(a) (b) (c)

Figure 2. The measured images from our system using polystyrene bead: (a), (b) measured images of a polystyrene bead (in white boxed A and A') and a homogeneous background field (in white boxed B and B') from the reference arm (I_R) and the object arm (I_O), respectively, and (c) generated double interferogram ($I_O + I_R$) at detector plane corresponding to (a) and (b); The white solid and dashed line boxes are corresponding to object and reference images, respectively.

both conditions, can be implemented by a pair of objective lenses.[9] The eDOF optics in our system can be illustrated as shown in Fig. 3. The specimen is placed at IP (image plane), and the conjugate image of the specimen is formed at IVP (immediate virtual plane). The MO3 with adapter lens (L3) delivers the image at IVP to detector. The simplified eDOF optics is mounting a simple mirror (M3) in Figs. 1(a)(b) for scanning of conjugate image at IVP. By moving M3, the focused plane of the specimen is remotely adjusted without moving the objective lens or specimen. Then, we can reduce a number of objective lenses. When MO2 is identical to MO1 in Figs. 1(a)(b) or Fig. 3, it satisfies the perfect imaging condition that occurs only in an imaging system with unity magnification. Even though the specification of MO1 is changed against MO2 according to the size or position of a sample, the eDOF system compensates for the spherical aberration much better than single objective lens imaging can.

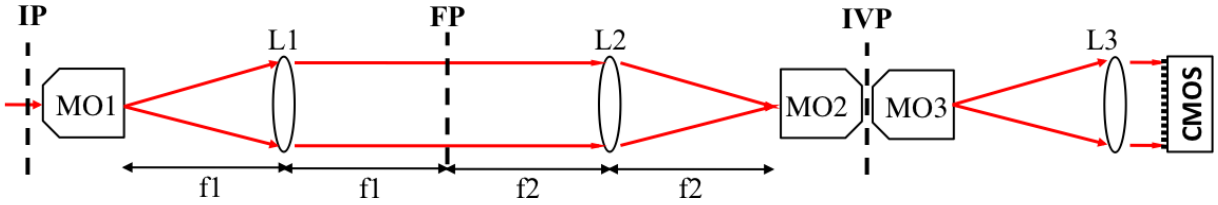

Figure 3. The basis eDOF optics for our system in Figs. 1(a)(b).

2.2 Measurements

We reconstruct the quantitative phase image of a sample using PSI and HPM setups. Generally, PSI and HPM reconstruct the quantitative phase image using multiple measurements and a single measurement, respectively. At the CMOS detector, the measurement is described as follows

$$I_i(x,y) = I_R(x,y)^2 + I_O(x,y)^2 + I_R(x,y)I_O(x,y)\cos(q(x,y) + \Delta\phi(x,y) + \delta_i), \tag{1}$$

where $I_R(x,y)$ and $I_O(x,y)$ are the reference and object images, respectively; and $q(x,y)$ and $\Delta\phi(x,y)$ are spatial modulation frequency and phase difference between sample and background, respectively. By tilting the beam splitter (BS) or reflective optics in Figs. 1(a)(b), we can control the spatial modulation frequency $q(x,y)$. For PSI setup, we acquire the multiple phase shifted measurements with $\{\delta_i\}_{i=1}^4 = \{0, \frac{1}{2}\pi, \pi, \frac{3}{2}\pi\}$ using SLM and apply the four step algorithm[2] given as

$$\Delta\phi = \tan^{-1}\Big[\frac{I_4(x,y) - I_2(x,y)}{I_3(x,y) - I_1(x,y)}\Big]. \tag{2}$$

For HPM setup, the phase difference ($\Delta\phi$) is calculated based on Hilbert transform;[3]

$$G(x) = \frac{1}{2}\tilde{I}_1(x) + i\frac{P}{2\pi}\int \frac{\tilde{I}_1(x')}{x - x'}dx', \tag{3}$$

where $\delta_1 = 0$ in a single measurement. To acquire exact phase information from Eq. 3, the low frequency component in Eq. 1 is removed by high pass filtering, and using $G(x)$ the phase difference is calculated as follows

$$\Delta\phi = \tan^{-1}\Big\{\frac{Im[G(x)]}{Re[G(x)]}\Big\}. \tag{4}$$

In our HPM setup, we acquired the two phase measurements with slightly different phase shift (δ_i) from double interferogram due to the different position of a sample as shown in Fig. 2(c). Averaging two reconstruction results from double interferogram, we achieve the high signal-to-noise ratio (SNR) reconstruction result.

The calculated $\Delta\phi$ is wrapped phase image, since the arctan function returns between $-\pi \sim +\pi$. To acquire exact phase image, we apply the phase unwrapping algorithm,[10] and then remove the background by

2-D polynomial fitting. Then, using $\Delta\phi$ calculated from HPM and PSI, the thickness of a sample is defined from OPL definition;

$$h(x,y) = \Delta\phi \frac{\lambda}{2\pi\Delta n}, \tag{5}$$

where Δn is the refractive index difference, and $\Delta\phi$ is acquired from Eqs. 2 and 4.

3. RESULTS

To confirm the proposed method, we applied the HPM and PSI setups to various samples. First, we experiment the eDOF performance of our system using $3\mu m$ polystyrene beads (n=1.59, Fluka) as shown in Fig. 4. The polystyrene beads are mixed with poly(dimethylsiloxane) (PDMS), and then placed between two cover slides. The refractive index of PDMS is defined as 1.40.[11] To observe the polystyrene beads, we applied the 100× (NA=1.30) oil-immersed objective lens at MO1. Figure 4 illustrates the quantitative phase images of the polystyrene bead, which is located at various distances from the focal plane of the object lens (MO1) in Fig. 1(b). Then, the focal planes of polystyrene bead are adjusted moving M3 in the object arm without moving objective lens or specimen for various distances. We also plot the maximum height of the calculated phase images to demonstrate the reliability of phase measurement at various distances. The bright-field images by 100× objective lens (MO1) are blurred as image inset in Fig. 4. However, according to our measurements the height is about $3\mu m$ for every planes.

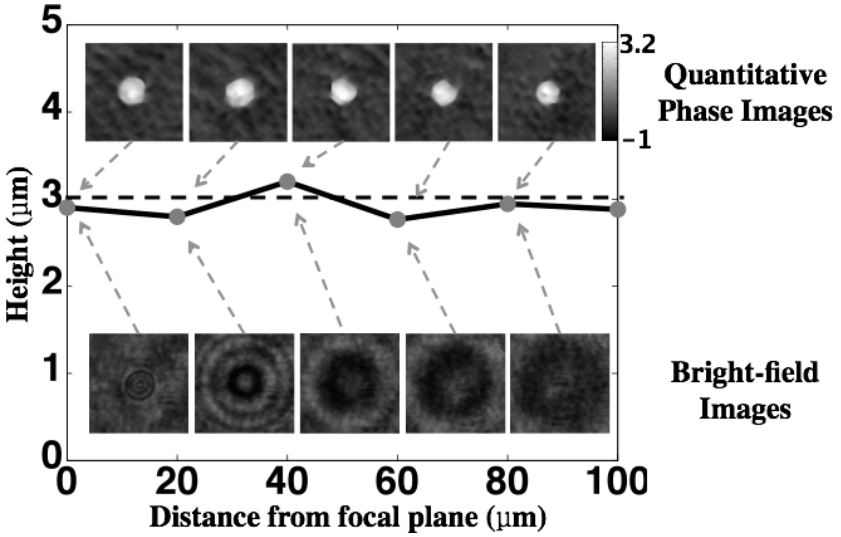

Figure 4. Calculated phase maps using our HPM setup. The measurements are obtained without moving objective lens or specimen, but rather by scanning the mirror in the object arm. The corresponding bright-field images show severe blurring.

We also applied our system for the monitoring of red blood cells (RBCs) in microfluidic devices. Note that a microfluidic device is commonly developed for cell culturing or as analysis, and that people are interested in real-time monitoring of samples,[12,13] since the staining process often disturbs the continuous cultivation or analysis of a cell for a prolonged period of time. The RBCs samples were obtained from the Republic of Korea National Red Cross Organization (Daejeon, Korea) in compliance with safety regulations. Using the aforementioned PSI and HPM methods, we acquired the phase image of RBCs as shown in Figs. 5 and 6. In Fig. 5(a), the FOV of specimen image contains the microchannel area with non-channelized area. RBCs diluted by phosphate buffered saline (PBS) solution are injected into the microchannel. Then, the black box area (denoted by A in Fig. 5(a)) above the microchannel is used as the reference field, whereas the black box area denoted by B corresponds to the specimen area in the microchannel. In PSI results, the phase map of the white box in Fig. 5(b) is shown

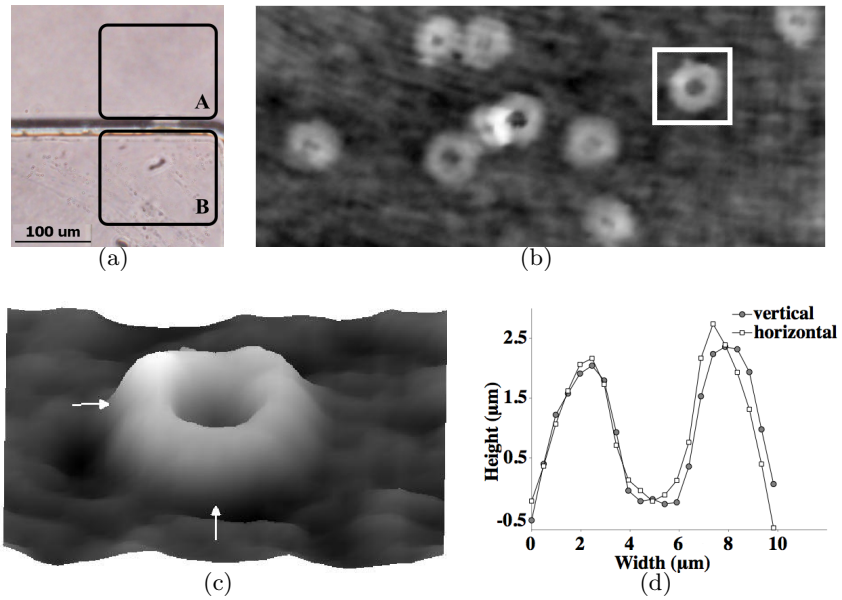

Figure 5. Experimental results of RBCs using PSI setup: (a) microfluidic device for RBCs, a 100μm scale bar is shown; (b) calculated phase image of the channel with RBCs, (c) 3-D profile of the RBCs within white box in (b), and (d) thickness measurements at horizontal and vertical arrow directions in (c).

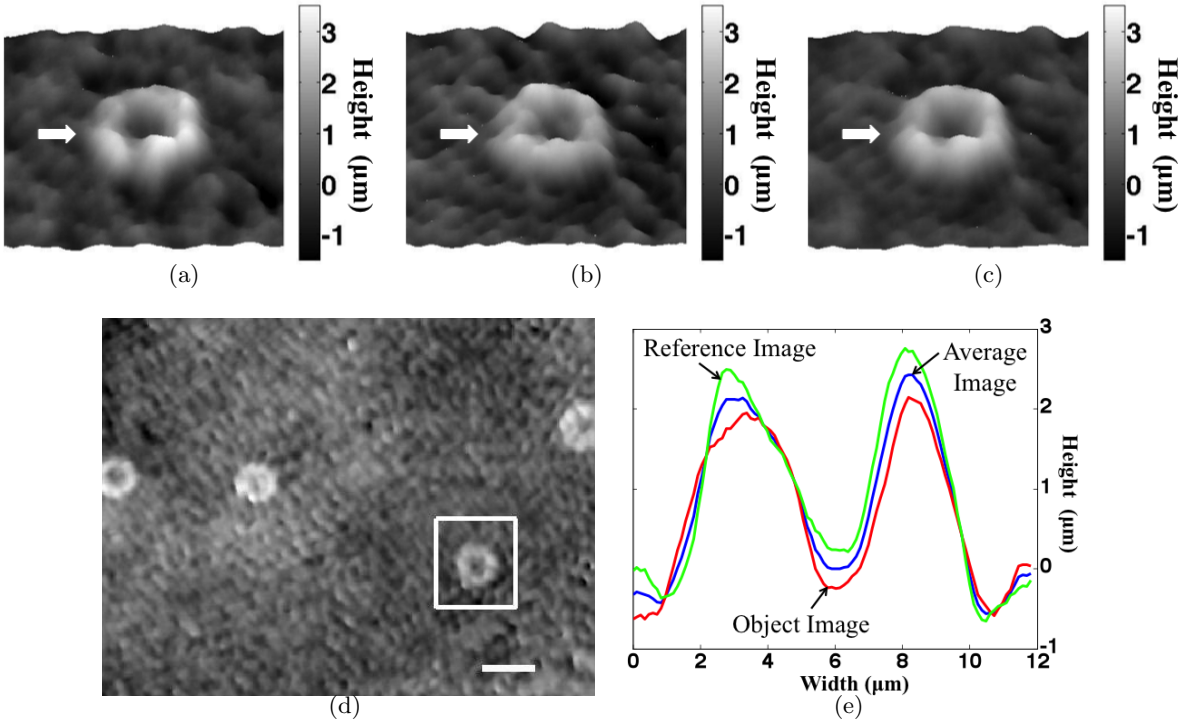

Figure 6. Experimental results of RBCs using HPM setup: (a), (b) quantitative phase images from the object and reference images, (c) quantitative phase image from averaging of (a) and (b), (d) a typical phase image from HPM measurement; a 10μm scale bar is shown, and (e) thickness measurements of the arrow directions in (a), (b), and (c).

in Fig. 5(c). The thickness profiles in Fig. 5(c) along two arrow directions are shown in Fig. 5(d). In HPM results, Figs. 6(a)(b) illustrate the reconstruction results using the measurement of sample and reference areas, respectively, whereas Fig. 6(d) illustrates the thickness profiles along the arrow directions in Figs. 6(a)-(c). Due to the averaging, the phase noise is significantly reduced in Fig. 6(c). The refractive index of the surrounding media and the RBCs were set to $n_m = 1.34$ and $n_{cell} = 1.40$, respectively.[14] The measured phase maps of the RBCs coincides with that found in the literatures (approximately $2\mu m$ in human).[3,6,15]

4. DISCUSSION

We developed a novel quantitative phase microscopy based on the eDOF. The modified Michelson interferometry splits the measured specimen image onto the reference arm and the object arm. The additional microscope objective lens switches the specimen image in the object arm, and then the homogenous background area in the specimen image was used as self-reference field. Simultaneously, a pair of objective lens increases the depth-of-field thanks to the eDOF optics. The quantitative phase image is acquired by use of phase shifting interferometry and Hilbert phase microscopy. Moreover, our system is suitable for microfluidic device, since the device has wide non-channelized area. The proposed method is confirmed by polystyrene beads and red blood cells in microfluidic device.

ACKNOWLEDGMENTS

The authors would like to thank Myung Gwon Lee for handling PDMS and RBCs samples, respectively. This work is supported in part by Korea Science and Engineering Foundation (2009-0081089).

REFERENCES

[1] Murphy, D. B., [*Fundamentals of Light Microscopy and Electronic Imaging*], Wiley-Liss, 1st ed. (2001).

[2] Popescu, G., Deflores, L. P., Vaughan, J. C., Badizadegan, K., Iwai, H., Dasari, R. R., and Feld, M. S., "Fourier phase microscopy for investigation of biological structures and dynamics," *Opt. Lett.* **29**(21), 2503–2505 (2004).

[3] Ikeda, T., Popescu, G., Dasari, R. R., and Feld, M. S., "Hilbert phase microscopy for investigating fast dynamics in transparent systems," *Opt. Lett.* **30**(10), 1165–1167 (2005).

[4] Warger, II, W. C. and Dimarzio, C. A., "Computational signal-to-noise ratio analysis for optical quadrature microscopy," *Optics Express* **17**, 2400–2422 (2009).

[5] Marquet, P., Rappaz, B., Magistretti, P. J., Cuche, E., Emery, Y., Colomb, T., and Depeursinge, C., "Digital holographic microscopy: a noninvasive contrast imaging technique allowing quantitative visualization of living cells with subwavelength axial accuracy," *Opt. Lett.* **30**(5), 468–470 (2005).

[6] Popescu, G., Ikeda, T., Dasari, R. R., and Feld, M. S., "Diffraction phase microscopy for quantifying cell structure and dynamics," *Opt. Lett.* **31**(6), 775–777 (2006).

[7] Su, Y.-D., Chen, S.-J., and Yeh, T.-L., "Common-path phase-shift interferometry surface plasmon resonance imaging system," *Opt. Lett.* **30**(12), 1488–1490 (2005).

[8] Botcherby, E., Juskaitis, R., Booth, M., and Wilson, T., "An optical technique for remote focusing in microscopy," *Optics Communications* **281**(4), 880 – 887 (2008).

[9] Botcherby, E. J., Juskaitis, R., Booth, M. J., and Wilson, T., "Aberration-free optical refocusing in high numerical aperture microscopy," *Opt. Lett.* **32**(14), 2007–2009 (2007).

[10] Valadão, G. and Bioucas-Dias, J., "CAPE: combinatorial absolute phase estimation," *J. Opt. Soc. Am. A* **26**(9), 2093–2106 (2009).

[11] Bliss, C. L., McMullin, J. N., and Backhouse, C. J., "Rapid fabrication of a microfluidic device with integrated optical waveguides for DNA fragment analysis," *Lab Chip* **7**, 1280–1287 (2007).

[12] El-Ali, J., Sorger, P. K., and Jensen, K. F., "Cells on chips," *Nature* **442**, 403–411 (2006).

[13] Dittrich, P. S. and Manz, A., "Lab-on-a-chip: microfluidics in drug discovery," *Nat Rev Drug Discov* **5**, 210–218 (2006).

[14] Lee, S., Lee, J. Y., Yang, W., and Kim, D. Y., "Autofocusing and edge detection schemes in cell volume measurements with quantitative phase microscopy," *Opt. Express* **17**(8), 6476–6486 (2009).

[15] Karlsson, A., He, J., Swartling, J., and Andersson-Engels, S., "Numerical simulations of light scattering by red blood cells," *IEEE Transactions on Biomedical Engineering* **52**(1), 13–18 (2005).